JCI The Journal of Clinical Investigation

Intrinsic endothelial hyper-responsiveness to inflammatory mediators drives acute episodes in models of Clarkson disease

Ararat J. Ablooglu, … , Samir M. Parikh, Kirk M. Druey

J Clin Invest. 2024. https://doi.org/10.1172/JCI169137.

Research In-Press Preview **Vascular biology**

Clarkson disease (monoclonal gammopathy-associated idiopathic systemic capillary leak syndrome, ISCLS) is a rare, relapsing-remitting disorder featuring the abrupt extravasation of fluids and proteins into peripheral tissues, which in turn leads to hypotensive shock, severe hemoconcentration, and hypoalbuminemia. Specific leakage factor(s) and pathways in ISCLS are unknown, and there is no effective treatment for acute flares. Here we characterize an autonomous vascular endothelial defect in ISCLS that is recapitulated in patient-derived endothelial cells (ECs) in culture and in a mouse model of disease. ISCLS-derived ECs are functionally hyper-responsive to permeability-inducing factors like VEGF and histamine in part due to increased endothelial nitric oxide synthase (eNOS) activity. eNOS blockade by administration of N(γ)-nitro-L-arginine methyl ester (L-NAME) ameliorates vascular leakage in an SJL/J mouse model of ISCLS induced by histamine or VEGF challenge. eNOS mislocalization and decreased protein phosphatase 2A (PP2A) expression may contribute to eNOS hyper-activation in ISCLS-derived ECs. Our findings provide mechanistic insights into microvascular barrier dysfunction in ISCLS and highlight a potential therapeutic approach.

Intrinsic endothelial hyper-responsiveness to inflammatory mediators drives acute episodes in models of Clarkson disease

Ararat J. Ablooglu[1], Wei-Sheng Chen[1], Zhihui Xie[1], Abhishek Desai[1], Subrata Paul[2], Justin B. Lack[2], Linda A. Scott[1], A. Robin Eisch[1], Arkadiusz Z. Dudek[3], Samir M. Parikh[4], Kirk M. Druey[1*]

[1]Lung and Vascular Inflammation Section, Laboratory of Allergic Diseases, National, Institute of Allergy and Infectious Diseases/National Institutes of Health, (NIAID/NIH), Bethesda, MD, 20892, USA

[2]Integrative Data Sciences Section, NIAID/NIH, Health, Bethesda, MD, 20892, USA.

[3]Division of Medical Oncology, Mayo Clinic, Rochester, MN 55902

[4]Division of Nephrology, Departments of Internal Medicine and Pharmacology, University of Texas Southwestern Medical Center, Dallas, TX, 75225, USA

Correspondence: 10 Center Drive, Room 11N238A, Bethesda, MD, 20892, USA; kdruey@niaid.nih.gov; 301-435-8875

Conflict of interest statement
The authors have declared that no conflict of interest exists.

Keywords: vascular leakage, endothelium, monoclonal gammopathy, nitric oxide

Abstract

Clarkson disease (monoclonal gammopathy-associated idiopathic systemic capillary leak syndrome, ISCLS) is a rare, relapsing-remitting disorder featuring the abrupt extravasation of fluids and proteins into peripheral tissues, which in turn leads to hypotensive shock, severe hemoconcentration, and hypoalbuminemia. Specific leakage factor(s) and pathways in ISCLS are unknown, and there is no effective treatment for acute flares. Here we characterize an autonomous vascular endothelial defect in ISCLS that is recapitulated in patient-derived endothelial cells (ECs) in culture and in a mouse model of disease. ISCLS-derived ECs are functionally hyper-responsive to permeability-inducing factors like VEGF and histamine in part due to increased endothelial nitric oxide synthase (eNOS) activity. eNOS blockade by administration of N(gamma)-nitro-L-arginine methyl ester (L-NAME) ameliorates vascular leakage in an SJL/J mouse model of ISCLS induced by histamine or VEGF challenge. eNOS mislocalization and decreased protein

phosphatase 2A (PP2A) expression may contribute to eNOS hyper-activation in ISCLS-derived ECs. Our findings provide mechanistic insights into microvascular barrier dysfunction in ISCLS and highlight a potential therapeutic approach.

Introduction

The initial presentation of ISCLS is frequently complicated by multiple organ dysfunction syndrome (MODS), rhabdomyolysis, and intravascular thrombosis (1, 2). Compartment syndrome may occur in the extremities due to excessive administration of intravenous fluids, frequently necessitating fasciotomies and/or limb amputation. Vascular leakage ultimately recedes spontaneously, typically after several days, which is followed by the mobilization of extravasated fluids into the circulation in a "post-leak" phase. During this period, patients are at

high risk for flash pulmonary edema due to cardiac dysfunction. Between episodes, patients show no overt pathological phenotype. Mortality during ISCLS flares approaches 30%, in part because no acute intervention has been proven to shorten the duration of episodes or prevent complications (1). By contrast, monthly prophylaxis with high dose intravenous immunoglobulins (IVIG) substantially reduces the frequency and severity of ISCLS flares and increases survival (3-5).

The mechanism by which IVIG prevents ISCLS relapse is unknown. Most ISCLS flares are triggered by antecedent infections such as viral upper respiratory infections (including COVID-19), suggesting a role for inflammation in the induction of vascular leak (1, 6). However, extensive proteomic profiling of acute ISCLS sera has not yet uncovered unique humoral factor(s) that may trigger attacks (7, 8). More than 90% of patients with ISCLS have a monoclonal gammopathy of unknown significance (MGUS, typically IgG kappa), but its role in disease pathogenesis is unknown (5).

While fewer than 500 cases of ISCLS have been described in the medical literature (9), we have assembled the world's largest ISCLS registry (>80 patients with a confirmed diagnosis), and our previous studies point to microvascular dysregulation in this disease. Patients challenged intradermally with permeability provocateurs (morphine or histamine) have increased vascular leakage compared to healthy controls, as evidenced the increased size of skin "wheals" due to localized edema (10). Blood-outgrowth endothelial cells (BOECs) expanded from asymptomatic patients with ISCLS have gene expression patterns that differ significantly from those in cells from healthy controls (8, 11). In a mouse model of ISCLS induced by systemic histamine challenge, SJL/J mice are uniquely susceptible to vascular leakage and mortality compared to most other inbred strains (10, 12). This autosomal recessive trait, termed *Histh*, maps to a

quantitative trait locus on Chr6 that is syntenic to the locus most closely aligned with ISCLS in a human genomic association study (Chr3.25p) (13).

Based on these findings suggestive of vascular hypersensitivity, we hypothesized that acute ISCLS flares are initiated by an autonomous endothelial defect characterized by exaggerated barrier dysfunction in response to pro-inflammatory mediators. To test this, we examined the morphology and functional behavior of the microvasculature of patients in situ and in BOECs ex vivo. Patient-derived ECs were hyper-responsive to several mediators of permeability in an eNOS-dependent fashion. Inhibition of eNOS ameliorated vascular leakage in the SJL/J mouse model of ISCLS, suggesting a therapeutic approach to acute disease flares.

Results

The endothelial response to histamine is exaggerated in patients with ISCLS

Intradermal challenge with unrelated leak-inducing agents (histamine and morphine) elicits significantly more focal skin edema in patients with ISCLS than in controls (10). To determine the cellular and molecular mechanisms underlying this observation, we used

129 immunofluorescence to quantify extravasation of the serum protein fibrinogen in fixed skin
130 biopsies from challenged patients (14). Demographic information about patients and healthy
131 controls is shown in **Supplemental Table 1**. The ISCLS group was significantly older (albeit
132 with a similar range) and trended more male and whiter than the control the control group. A
133 solid majority of the patients with ISCLS had MGUS whereas none of the controls did. The
134 endothelial marker CD31 was used to quantify vascular area of the skin. As expected, little to no
135 fibrinogen immunostaining was seen in saline-challenged skin whereas we detected abundant
136 extravascular fibrinogen at the histamine-challenged sites (**Figure 1A**). The extravascular
137 fibrinogen^{+} area was significantly greater in histamine-challenged skin of patients with ISCLS
138 compared to that in healthy controls (**Figures 1A-B**). Baseline serum fibrinogen levels did not
139 differ between the groups (**Supplemental Figure 1**). Since histamine acts directly on H1
140 receptors expressed on ECs (15), these results suggested an increased functional response to
141 histamine in the ISCLS endothelium.
142 Neither vasculitis nor aberrant angiogenesis has been observed consistently in biopsies of
143 skin or skeletal muscle taken from patients during ISCLS flares (9, 16). We did not find evidence
144 of cellular inflammation or other histological abnormalities in the skin of asymptomatic patients
145 by light microscopy (**Supplemental Figure 2**). Dropout of pericytes, smooth muscle-like cells
146 that line microvessels, has been associated with endothelial hyper-permeability (17, 18).
147 However, we detected equivalent pericyte coverage (immunoreactive smooth muscle α actin) of
148 microvessels in ISCLS and control biopsies (**Figures 1C-D**). Likewise, aberrant expression or
149 interaction of extracellular matrix components such as collagen IV with integrins expressed on
150 ECs regulates vascular barrier function (19, 20). However, collagen IV immunostaining around
151 vessels in ISCLS and healthy control skin did not differ from one another (**Figure 1E-F**). These

findings further support the hypothesis that an exaggerated response to proinflammatory mediators, rather than underlying structural defects in the microvasculature, likely underlies vascular leakage during acute ISCLS flares.

Disruption of adherens junctions in ISCLS dermal microvascular endothelium

Application of acute, but not convalescent, ISCLS sera to normal dermal microvascular ECs induces transient barrier disruption—but not apoptosis, injury, or activation—through mechanisms that include disruption of adhesion junctions and cytoskeletal rearrangements that promote endothelial cell contraction (21, 22). To determine the molecular mechanisms involved in histamine-evoked vascular leakage in ISCLS skin, we quantified the expression of VE-cadherin, an essential mediator of endothelial intercellular adhesion, in skin biopsies. As expected, histamine challenge reduced VE-cadherin expression in skin of both groups compared to skin injected with saline alone (**Figure 2A**). However, the VE-cadherin^{+} area in skin microvasculature was already lower at baseline in patients with ISCLS than in controls and decreased further following histamine challenge (**Figure 2B**).

Pro-inflammatory mediators including histamine, bradykinin, and VEGF induce Src-mediated tyrosine phosphorylation of VE-cadherin on Tyr^{685}, which is required for internalization and the dissolution of adherens junctions (23). To assess the extent of VE-cadherin phosphorylation in skin biopsies, we assessed VE-cadherin (p-Tyr^{685}) in skin biopsies by immunofluorescence. We first evaluated the specificity of a VE-cadherin (p-Tyr^{685}) antibody used previously for immunostaining (24). We detected substantially reduced amounts of phospho-and total VE-cadherin in lysates from BOECs transfected with VE-cadherin targeted siRNA immunoprecipitated with VE-cadherin antibody compared to controls, confirming its

specificity (**Supplemental Figure 3**). Using this antibody, we detected a significant increase in VE-cadherin (p-Tyr^{685}) immunostaining in histamine-challenged dermal blood vessels compared to those treated with saline, and the increase in ISCLS skin was nearly double that seen in healthy controls (**Figures 2C-D**). Moreover, there was a significant correlation between VE-cadherin (p-Tyr^{685}) and fibrinogen extravasation (**Figure 2E**). Our findings thus far suggested that dermal microvasculature in ISCLS has impaired barrier function at homeostasis and after histamine challenge due to reduced VE-cadherin expression.

ISCLS-derived ECs exhibit durable hyper-responsiveness in vitro

To determine whether the increased permeability of ISCLS dermal microvasculature observed in situ was due to an autonomous endothelial defect, we systematically characterized the functional responses of patient-derived ECs to various mediators ex vivo. For these studies, we used BOECs expanded from blood of patients and healthy controls over multiple passages. BOECs have an endothelial morphology when visualized by light microscopy, form confluent monolayers (11) (**Supplemental Figure 4A**), and were uniformly CD31^{+}CD45^{-} as expected (25). CD31 expression was comparable in BOECs from patients with ISCLS and healthy controls (**Supplemental Figures 4B-D**).

We used electric cell impedance sensing (ECIS) to assess trans-endothelial resistance (TER) in real time through measurements of paracellular passage of low frequency (4 kHz) current. Whereas baseline resistance was comparable in ISCLS-derived or control BOECs, TER decreased significantly more and recovered more slowly in ISCLS BOECs stimulated with histamine (**Figures 3A-C**) or VEGF (**Figures 3D-F**). Thrombin induced a comparable drop in resistance and recovery in ISCLS and control BOECs, even at submaximal concentrations (**Figures 3G-I**).

Next, we examined dynamic changes in endothelial morphology that might account for the functional hyper-responsiveness. Untreated control and ISCLS BOECs had comparable membrane associated VE-cadherin expression and cortical actin (**Figure 4A**). Histamine or VEGF elicited paracellular gap formation, decreased VE-cadherin localization at intercellular junctions, and F-actin rearrangements (reduced cortical actin and increased planar actin stress fibers) compared to untreated cells as expected. In line with the responses of ISCLS skin microvasculature, the loss of membrane associated VE-cadherin expression was significantly more prominent in histamine- or VEGF-treated ISCLS BOECs than in control cells (**Figure 4B**). These findings support the hypothesis that functional defects in the ISCLS endothelium in response to permeability-inducing factors may be sufficient to account for the vascular hyper-responsiveness observed in situ.

Increased eNOS phosphorylation in ISCLS-derived BOECs

We next investigated the mechanisms contributing to increased permeability of the ISCLS endothelium. Expression of VEGFA (VEGFR2) and histamine (H1) receptors, key signaling proteins (eNOS, VE-cadherin), or transcripts for *CDH5* (encoding VE-cadherin) or *NOS3* (encoding eNOS) was comparable in control and ISCLS BOECs (**Figures 5A-C**). These results suggested that dysregulation of downstream intracellular signaling pathways might underlie the amplified functional responses of ISCLS-derived BOECs. Because we have previously detected elevated VEGF levels in acute ISCLS sera (21, 26), we focused specifically on the mechanisms underlying VEGF-induced hyper-permeability. VEGFR2-mediated signaling in several types of ECs hinges on activation of multiple effectors including Src, phosphatidylinositol 3-kinase (PI3K), and phospholipase Cγ1 (PLCγ1) (27). VEGF-induced increases in cytosolic Ca^{2+} (due to PLCγ1 activation) were similar in control and ISCLS BOECs (**Figure 5D**). Ca^{2+} flux elicited by

histamine or ionomycin was also equivalent in ISCLS and control BOECs (**Supplemental Figures 5A-B**). Unexpectedly, basal Akt phosphorylation (indicative of PI3K activation) was prominent in both control and ISCLS-derived BOECs to a comparable extent, and VEGF treatment did not elicit a significant increase in pAkt in either cell type (**Supplemental Figures 6A-B**). Although the mechanisms underlying these results require further study, they nonetheless suggested that increased PI3K activation does not contribute to the hyper-responsiveness of ISCLS-derived BOECs to VEGF.

To identify other perturbations in ISCLS cells, we conducted a phosphoproteomic screen. Among the most differentially phosphorylated proteins in VEGF-stimulated ISCLS-derived BOECs compared to controls were eNOS ($pSer^{1177}$, 2.3-fold higher), AMP kinase (AMPK, $pThr^{172}$), and beta-catenin (**Supplemental Figure 7**). In immunoblots of BOEC lysates from individual subjects, baseline and VEGF-stimulated eNOS phosphorylation were significantly increased in ISCLS BOECs compared to controls (**Figures 5E-F**).

Previous studies have demonstrated that eNOS activation is critical for histamine and VEGF-induced vascular leakage in ECs in vitro and in mice (28). To determine the role of increased eNOS phosphorylation in the impaired barrier function of ISCLS-derived BOECs, we transfected cells with eNOS-specific siRNA, which reduced eNOS protein levels more than 80% compared to cells transfected with a control siRNA (**Figures 5G-H**). While knockdown of eNOS attenuated the VEGF-evoked decrease in TER in both control and ISCLS-derived BOECs (**Figure 5I**), the responses of ISCLS-derived cells were inhibited to a significantly greater extent (**Figure 5J**). These findings suggest that the hyper-responsiveness of ISCLS ECs to VEGF is uniquely eNOS-dependent.

eNOS blockade mitigates vascular leakage in a mouse model of ISCLS

Like adult patients with ISCLS, aged (>6 months of age) SJL/J mice have no overt baseline vascular phenotype but are unusually susceptible to histamine challenge. Low doses of histamine (2.5 mg/kg) elicit vascular leakage in SJL/J mice, most prominently in peripheral tissues like skin and skeletal muscle (10). In contrast, much higher doses of histamine (1-2.5 log-fold) are typically required to induce vascular leakage in most inbred mouse strains including C57BL/6 (29-32). In our previous study, we observed that a high proportion of SJL/J mice die within 30 minutes of systemic challenge with histamine at doses as low as 10 mg/kg, unlike >20 other strains tested (10, 12). The genetic and phenotypic similarity of the Histh trait to the vascular hypersensitivity observed in patients with ISCLS suggests shared pathophysiological mechanisms.

To characterize the contribution of eNOS to vascular leakage in this ISCLS model, we treated aged SJL/J mice with the competitive eNOS inhibitor L-NAME prior to systemic challenge with low doses of histamine and measured Evans blue (EB) extravasation in peripheral tissues with a specific focus on skeletal muscle, which is the predominant site of vascular leakage in patients (**Figure 6A**). L-NAME prophylaxis significantly attenuated EB extravasation in muscle and stomach of histamine-challenged mice compared to vehicle alone (**Figures 6B-C**). Serum EB levels were comparable in PBS- or L-NAME-pretreated mice (**Figure 6D**). By contrast, this low dose of histamine elicited significantly less EB extravasation in muscle from histamine resistant mice (aged matched C57BL/6J) (12), and L-NAME pretreatment had no impact on the response (**Figure 6E and Supplemental Figure 8**). To evaluate the effect of L-NAME on the in vivo responses to an ISCLS-related cytokine, we measured EB extravasation in the skin of SJL/J mice after intradermal injection with VEGF (**Figure 6F**). L-NAME pretreatment significantly reduced EB content in VEGF-challenged skin compared to controls

(**Figures 6G-H**) but not in serum (**Figure 6I**). These findings suggest a unique and important role of eNOS in the pathophysiology of vascular leakage in the Histh model of ISCLS.

Mechanisms underlying increased eNOS activity in ISCLS ECs

We explored the potential causes of increased VEGF-induced eNOS phosphorylation in ISCLS-derived BOECs. VEGF activates several kinases that have the capacity to phosphorylate eNOS, including Akt and AGC protein kinases (e.g. AMPK) (28). Although the contribution of Akt to the hyper-reactivity of ISCLS-derived BOECs is unclear as noted above, AMPK phosphorylation was significantly increased in VEGF-treated ISCLS BOECs compared to control cells (**Figures 7A-B**).

Although AMPK has a well-established function as a sensor of increased intracellular AMP levels, previous studies of its role in endothelial permeability have yielded conflicting results (33, 34). Currently available chemical inhibitors of AMPK (e.g. Compound C) display considerable non-specificity in cells (35, 36), and we could not achieve robust knockdown of AMPK protein expression in BOECs by RNAi. AMPK is activated by several upstream kinases including Ca^{2+}-calmodulin dependent kinase kinase beta (CAMKKβ). To clarify the impact of AMPK on hyper-responsiveness due to eNOS activation in BOECs, we exposed cells to STO-609, a specific inhibitor of CAMKKβ. Although pretreatment with STO-609 completely blocked VEGF-induced AMPK phosphorylation (**Figures 7C-D**), it had no effect on VEGF-induced barrier dysfunction (**Figures 7E-F**) or eNOS phosphorylation (**Figures 7G-H**) in either ISCLS-derived or control BOECs. These findings suggest that AMPK does not contribute to eNOS hyper-activation in ISCLS-derived BOECs.

297 Because we were unable to clearly identify causative perturbations in the most well-
298 characterized VEGF-stimulated signaling pathways upstream of eNOS in ISCLS-derived
299 BOECs, we considered the possibility of aberrant subcellular eNOS localization. Published
300 studies have demonstrated that eNOS/p-eNOS localize predominantly at the cytoplasmic face of
301 the Golgi in ECs, with a smaller fraction at the plasma membrane (PM) (37, 38). In both ISCLS-
302 derived and control BOECs, we observed p-eNOS/eNOS immunostaining primarily in the
303 perinuclear region, consistent with Golgi localization, with a smaller fraction at the PM (**Figures**
304 **8A-B**). However, there were large clusters of PM-associated eNOS/p-eNOS in ISCLS-derived
305 BOECs in the presence or absence of VEGF stimulation that were absent in control cells
306 (**Figures 8A-B, Supplemental Movies 1-2**).
307 Beyond a potential role of eNOS mislocalization, we hypothesized that aberrant expression
308 and/or function of intracellular regulators of eNOS activity might also contribute to the observed
309 functional hyper-responsiveness of ISCLS-derived BOECs. Results from whole genome
310 sequencing done on 55 patients revealed ISCLS-associated previously unreported or highly rare
311 single nucleotide polymorphisms (SNPs) within the coding regions of several relevant genes
312 including *NOS3* itself (encoding eNOS), *ATP2B2* (39), and *PPP2R1B*, several of which were
313 predicted to be deleterious (CADD score >10) (**Supplemental Table 2**). Because total eNOS
314 expression was similar in ISCLS-derived BOECs and controls while p-eNOS was increased even
315 in quiescent cells, we focused further attention on candidate phosphatases. PP2A has a central
316 function in the dephosphorylation of eNOS on Ser^{1177} (40), and our previous results from RNA-
317 Seq performed on a smaller subset of BOECs suggested decreased expression of PP2A-encoding
318 genes including *PPP2R1B*, *PPP2R3A*, and *PPP2R5A* in ISCLS compared to controls (8). PP2A
319 is a Ser/Thr phosphatase consisting of core catalytic (C), scaffold (A), and variable regulatory

(B) subunits, and the structural subunits are required for full activity of the enzyme (41). We observed significantly less PP2A-Aβ (encoded by *PPP2R1B*) protein expression in ISCLS-derived BOECs than in controls while expression of PP2A-B and PP2A-C subunits was similar (**Figures 8C-D**). By contrast, *PPP2R1B* mRNA expression did not differ between control and ISCLS-derived BOECs, suggesting that the aberrant PP2A-Aβ expression resulted from post-transcriptional mechanisms (**Figure 8E**). Overexpression of FLAG-PP2A-Aβ in ISCLS-derived BOECs significantly reduced VEGF-induced barrier disruption (**Figures 8F-H**) and eNOS phosphorylation (**Figure 8I-J**). These results suggest that reduced PP2A-A expression contributes to the hyper-responsiveness of ISCLS ECs to VEGF.

Discussion

ISCLS is both rare and cryptogenic. Because the acute presentation resembles several more common conditions (e.g. sepsis) and unique biomarkers or diagnostic genetic assays do not yet exist, the diagnosis is frequently missed and/or delayed, with devastating consequences (1). Even in patients with an established diagnosis, clinicians are unable to determine when ISCLS will flare in each patient or predict how severe a given flare will be. The frequency of ISCLS attacks

varies widely, and effective interventions for acute episodes are non-existent. By examining vascular leakage in patients in situ, the molecular and biophysical behavior of cultured ECs in vitro, and a mouse model of disease, we discovered that an autonomous functional defect within the endothelium characterized by eNOS-dependent cytokine hypersensitivity may contribute to acute ISCLS crises.

Patients with ISCLS are typically asymptomatic between episodes and have normal physical exam findings. However, although we found no overt structural anomalies in the skin microvasculature in asymptomatic patients, VE-cadherin expression was reduced, suggesting the presence of ongoing, yet subclinical, endothelial dysfunction. This phenotype was partially recapitulated in ISCLS-derived BOECs, which displayed normal growth and morphology but had markedly exaggerated loss of intercellular adhesion when challenged with VEGF or histamine. Thus, the ISCLS endothelium may be primed for excessive leakage in the context of inflammation. Our findings also argue against a prominent role of endothelial cell injury or death in ISCLS-associated vascular leakage. We have not detected increased circulating levels of endothelial injury markers in acute ISCLS plasma (8), nor have we observed tissue hemorrhage in patients like that which can occur in infections with the Ebola/Marburg family of filoviruses due to direct endothelial cytotoxicity (42).

That the functional endothelial defect persists after passaging further suggests that the susceptibility of ISCLS-derived ECs to cytokine hypersensitivity is durable and raises the possibility of a genetic abnormality underlying the stress-induced endothelial phenotype. Although related studies of more common conditions have proposed that genetically determined variance in the host vascular response may contribute to the risk for other leakage pathologies (e.g., sepsis) (43-45), to our knowledge there is no known hyperpermeability disorder in which

366 the vasculature is genetically (or epigenetically) programmed to “hyper-respond” to otherwise
367 routine stimuli.

368 One possible exception was reported about a boy with recurrent episodes of vascular leakage
369 resembling ISCLS (one fatal) associated with a monoallelic loss-of-function (LOF) mutations
370 (D762V) in *ARHGAP5*, which encodes a GTPase activating protein for RhoB (p190BRhoGAP)
371 that is expressed in ECs (46). However, it is unlikely that this child had Clarkson disease
372 considering that the clinical presentation was atypical (cerebral and pulmonary edema and
373 hemorrhage, lack of peripheral edema or MGUS). Although dermal ECs isolated from this child
374 post-mortem recovered more slowly to TNFα-induced barrier disruption, they had normal
375 responses to histamine, unlike BOECs derived from adults with ISCLS. Moreover, this allele
376 was not detected in our NIH ISCLS cohort, nor did we consistently detect other previously
377 unreported or ultrarare LOF variants in *ARHGAP5*.

378 In fact, and consistent with the absence of familial inheritance of ISCLS, whole exome
379 sequencing performed on leukocyte DNA samples from seven pediatric probands with classic
380 ISCLS, their immediate relatives, and nine unrelated adults failed to identify any de novo,
381 previously unreported (or even highly rare) single nucleotide variants shared among any two
382 patients (47). Ultra-rare mutations in non-coding DNA or mosaicism could nonetheless
383 contribute to the pathogenesis of ISCLS. Simultaneous whole genome sequencing of endothelial
384 cell lines and unrelated tissues may be needed to detect low-frequency somatic variants confined
385 to the endothelium.

386 Our mechanistic studies point to an important contribution of eNOS dysregulation in the
387 pathogenesis of ISCLS. eNOS promotes endothelial barrier dysfunction through several
388 mechanisms including enhancement of Src-dependent phosphorylation of VE-cadherin on Tyr^{685}

389 in response to VEGF (48). Consistent with this mechanism, we detected increased VE-cadherin
390 (p-Tyr^{685}) in histamine-challenged ISCLS skin vasculature compared to controls. The
391 aggregation of p-eNOS at the PM of ISCLS BOECs could signify an underlying commitment to
392 leakage and increased sensitivity to agonists. Published studies of subcellular localization in
393 HUVECs demonstrate that eNOS is acylated and localizes predominantly at the PM within
394 caveolae and on the cytoplasmic side of the Golgi membrane (28). Studies of *Nos3-/-* ECs
395 reconstituted with differentially localized eNOS mutants have further suggested that PM-targeted
396 eNOS is constitutively phosphorylated on Ser^{1177} and produces more NO than a Golgi-targeted
397 mutant in response to Ca^{2+}- or Akt-activating stimuli (49). Since caveolin-1 is a negative
398 regulator of eNOS activity (50), it may be informative to determine whether these eNOS
399 aggregates are excluded from PM-associated caveolin-rich microdomains in ISCLS-derived
400 BOECs.
401 The significance of increased AMPK phosphorylation in ISCLS BOECs is unclear. Our
402 results are in line with those from earlier studies of human umbilical vein-derived ECs
403 (HUVECs) and lung ECs from *Ampkα1-/-* mice, which have intact VEGF-induced eNOS
404 phosphorylation (33). However, more recent studies of brain microvascular cells and mouse
405 retinae ex vivo have pointed to an indispensable role for AMPK in VEGF- and bradykinin-
406 evoked permeability downstream of Ca^{2+} and CAMKKβ (34). The function of AMPK in
407 permeability may thus vary with endothelial heterogeneity. Increased AMPK activity in
408 quiescent ISCLS ECs also raises the specter of a metabolic phenotype reflective of an increased
409 intracellular AMP:ATP ratio; further examination of ISCLS BOEC metabolism in the presence
410 or absence of inflammatory stimuli may be warranted.

Last, we detected reduced PP2A-A expression in ISCLS BOECs, which may in turn augment and/or prolong eNOS activity. PP2A-A knockdown by RNAi destabilizes expression of B and C subunits and thereby compromises PP2A enzymatic activity (51). Somatic mutations in *PPP2R1A* and *PPP2R1B* are frequently detected in cancer, and functional haploinsufficiency promotes tumorigenesis (52). We did not detect any well-known cancer-associated variants in PP2A-A or PP2A-B encoding genes in ISCLS, and thus further studies are required to determine the significance of *PP2R1A-B* mutations for PP2A-A expression in ISCLS.

Our discovery of endothelial hypersensitivity in ISCLS has significant implications for the treatment of acute attacks. Although ISCLS flares are frequently triggered by viral infections and accompanied by transient increases in circulating proinflammatory and angiogenic cytokines (e.g. TNFα, CXCL10, CCL2, IL-6, VEGF, angiopoietin 2), the cytokine storm may have already peaked by the time the patient presents with hypotensive shock (21, 26). Consequently, inhibition of specific humoral factors or their receptors (histamine, VEGF, bradykinin) or more broadly active anti-inflammatory agents (e.g. corticosteroids, immunosuppressives) exerts no benefit on acute ISCLS crises (2, 53, 54). However, administration of methylene blue, a NO scavenger, was reported to reverse hypotension in a single patient (55). Further detailed characterization of the eNOS-dependent and -independent endothelial defect(s) in ISCLS-derived ECs may uncover new and more effective therapeutic targets.

Methods

Sex as a biological variable

The prevalence of ISCLS is similar in men and women; therefore, we did not consider sex as a biological variable. All available patient-derive cell lines regardless of sex were used. Approximately equal numbers of male and female mice were used for functional studies.

Reagents, chemicals, and antibodies

Collagen I, L-NAME, L-cysteine, Gelatin (from porcine skin), thrombin (from human plasma),

Histamine, Evans blue, STO-609, probenecid, and DAPI were from Sigma. Recombinant human VEGF165 was from PeproTech. Lipofectamine and phalloidin were purchased from ThermoFisher. Complete and PhoSTOP inhibitor tablets were from Roche. A full list of antibodies used is provided in **Supplemental Table 3**.

Isolation and expansion of BOECs

Peripheral blood mononuclear cells (PBMCs) were isolated from whole blood and cultured in Endothelial Growth Medium (EGM-2, Lonza) on collagen I-coated dishes as previously described (11). The culture medium was changed every other day for several weeks until discrete colonies formed, and BOECs were expanded according to published protocols (25). BOECs from anonymized healthy donors were used as controls for all studies, and cells were used up to 20 passages.

RNA interference

BOECs were transfected with the ON-TARGETplus SMARTpool siRNA for human *NOS3* (L-L-006490-00-0005) or control non-targeting siRNA (D-001810-10-20) (final concentration 12.5 nM) using Dharmafect transfection reagent 4 (Dharmacon). Expression and functional studies were done 72 hours after transfection.

Lentiviral transfection

Vector for the negative control virus (EX-NEG-Lv203) and virus preparation reagents were obtained from GeneCopoeia™. Virus was prepared with according to the manufacturer's instructions. Briefly, 2.5 μg DNA/EndoFectin complex (Lenti-Pac™ HIV expression packing kit cat. #LT001), diluted in Opti-MEM I medium (Gibco cat. #31985062), transfected into HEK293A cells. The next day, transfection medium was replaced with fresh DMEM and 1:500 (V/V) Titer Boost reagent. 48 hrs. post transfection pseudovirus-containing medium was harvested and concentrated with Lenti-X™ concentration solution (Takara) overnight at 4 °C (1:3, V/V). The virus pellet was resuspended in complete BOEC medium and stored in aliquots at -80 °C. BOECs were infected with FLAG-PPP2R1B virus (GeneCopoeia™, cat# EX-W0293-Lv203), or with negative control virus at confluence (1:120, V/V) in the presence of polybrene (8 μg/ml, #TR-1003-G, Millipore) for 2 hrs. at 4 °C and transferred to 37 °C. Cells were evaluated at 20-24 hours post infection.

Immunoblotting and immunofluorescence

Cell lysates were prepared in radioimmunoprecipitation buffer containing protease and phosphatase inhibitor cocktails and electrophoresed on NuPAGE gels (ThermoFisher Scientific) before transfer to nitrocellulose or polyvinylidene difluoride (PVDF) membranes. After immunoblotting, blots were with near-infrared–conjugated secondary antibodies using the Li-COR Odyssey 3000 imager (LI-COR Biosciences). Signals were quantified using ImageStudio (Li-Cor) or ImageJ software. For immunofluorescence, BOECs were grown to confluency on collagen I-coated Chamberwell slides (Nunc) and serum starved with 0.2% BSA in EBM-2 medium (5 hours, 37°C). Following stimulation, cells were fixed in 4% paraformaldehyde in PBS (15 min, room temperature [RT]) and permeabilized with 0.2% Triton X-100 in PBS (5 min., room temperature [RT]). After incubation in blocking buffer (3% BSA/0.1% Tween-20/5% goat serum in PBS, 1 hour, RT), cells were incubated with primary antibodies in blocking buffer overnight at 4°C. Cells were washed 4 times with wash buffer (0.1% Tween-20 in PBS),

followed by incubation with goat anti-mouse or anti-rabbit fluorophore-conjugated secondary antibodies in blocking buffer. Cells were then incubated with DAPI (1 μg/ml, Invitrogen) for 5 min at RT and mounted with glass coverslips using ProLong antifade mounting medium (Invitrogen). Skin sections were fixed in cold methanol and then stained blocked with Image-iT FX signal enhancer (Invitrogen) prior to incubation with antibodies and processing as above. Images were acquired at 63x magnification using a Leica DMI8 Sp8 confocal microscope.

For quantification of 3D rendered images of and skin biopsies and eNOS immunostaining in BOECs (Figure 1, Supplemental Movies 1-2), we used Imaris software for 3D rendering and volumetric measurement. We used multi-position tiling to obtain a larger or entire area of skin to observe a global view of the spatial distribution. For one dimensional images (Figure 2), we used Imaris and ImageJ to calculate the absolute fluorescence intensity or ratiometric analysis (% area), respectively. In experiments using cell monolayers (Figure 4), areas of VE-cadherin disruption on cell membranes were identified using Image J in >5 separate fields/condition for each experiment. We used the "Auto Threshold" function to first limit analysis of 8-bit images to positively stained areas. We obtained numerical values for total cell perimeter and identified all linear regions of the membrane lacking positive signal manually using the "freehand" tool. The final values (% membrane gaps) were calculated as the sum of non-stained areas divided by cell perimeter.

Ca^{2+} measurements

BOECs were plated in 96-well black-walled plates (1×10^5 cells/well). Ca^{2+} Fluo-6 indicator and (FLIPR Calcium 6 assay kit, Molecular Devices) and probenecid (1 mM) was added to each well containing serum-free EGM-2 for 2 hours. Agonists were added robotically to wells using the FlexStation III instrument (Molecular Devices), and fluorescence was measured every 1.5 seconds for 180 seconds. Each reading was divided by the initial value to obtain the normalized Ca^{2+} value.

Phosphoproteome profiling

A human Phospho-Kinase Array Kit was purchased from R&D Systems and analyzed according to the manufacturer's instructions. Briefly, BOECs were serum starved in EGM-2 for 5 hours prior to stimulation with VEGF (100 ng/mL) for 15 minutes. Cell lysates were prepared as above and incubated with membranes overnight at 4°C. Signals were detected and quantified as outlined for immunoblots.

ECIS

BOECs were plated on gelatin-coated wells (4×10^4 cells/well) containing gold plated electrodes (8W10E+ PET arrays, Applied BioPhysics). Electrodes were cleaned with cysteine (100 mM) overnight prior to coating. Cells were incubated overnight in EGM-2 followed by serum-starvation in Endothelial Basal Medium (Lonza) containing 0.2% BSA for 5 hours at 37°C prior to stimulation. TER was recorded over a period of 20 hours. Each condition was measured in duplicate in a single experiment and averaged. Absolute resistance values were normalized by subtracting the resistance at time zero (pre-treatment); the maximal change in resistance was calculated as percentage change over time zero.

Mouse ISCLS model

Aged (>6 months of age) SJL/J mice (Jackson Laboratories) were used to assess vascular leakage as previously described (10) and as outlined in Figures 6A and 6F. Briefly, mice were injected with 100 µl of 2% EB in PBS retro-orbitally. Immediately thereafter, mice were injected with 100 µl histamine in PBS (2.5 mg per kg body weight) intraperitoneally. 15 minutes post-injection, mice were deeply anesthetized by isoflurane inhalation and perfused with 5 ml of heparinized PBS through the left ventricle to remove residual intravascular EB. Tissues were harvested and heated at 95 °C for 1 hour to obtain dry weights of tissues. A Miles assay was performed to assess VEGF-induced vascular leakage in skin. Briefly, mice were injected intraperitoneally with pyrilamine maleate (4 mg/kg body weight, Sigma) 30 min prior to injection with EB dye to reduce background permeability during handling. Mice were then injected with EB via retro-orbital injection as before followed by intradermal injections of VEGF or saline (50 µl total volume). 30 minutes after the intradermal injection, the dorsal skin was collected with a 12-mm biopsy punch. EB was extracted from dried tissues with formamide (Sigma; 56 °C for 48 hrs.). The amount of EB in each sample was determined by measuring the absorbance at 620 nm, and results were expressed as EB dye amount (ng) per 100 mm^2 of skin or tissue weight (mg), with quantification against a standard curve.

Whole genome sequencing

Variants were called jointly using the publicly available genome-seek pipeline (https://github.com/OpenOmics/genome-seek). Briefly, raw fastq files were trimmed using fastp (56) and aligned with bwa-mem2 to the GRCh38 human genome reference. Samblaster version 0.1.26 (57) was used to flag PCR duplicates and BAM files were sorted using samtools v1.16.1 (58). Final BAM files were used as input to DeepVariant v1.4.0 (59) for generating gVCFs, and GLNexus v1.4.1 (60) was used to joint genotype the cohort. Variants were annotated with gnomAD (61) allele frequency and CADD (62) score using open cravat v2.2.5 (63). We used additional annotation tools including Loss/Gain Function Prediction software (https://itanlab.shinyapps.io/goflof/) (64) to predict variant functional impact.

Statistics

All statistical analyses were performed using GraphPad Prism. Unpaired, two-tailed Student's *t* tests were used to compared two groups, and non-parametric Mann Whitney tests were used for non-normally distributed data. Chi square tests were used to compare demographic contingency variables. One-sample *t* test was used to compare the differences between one sample and a normalized control (for example, to 100%). One- or two-way analysis of variance (ANOVA) was used for analysis of multiple groups, with the post hoc multiple comparisons tests recommended by Prism. Pearson coefficients were calculated to assess correlation between parameters. $p < 0.05$ was considered statistically significant.

Study approval

Patients with ISCLS were enrolled in a clinical study protocol approved by the Institutional Review Board of the National Institutes of Health (09-I-0184) after providing written informed consent. Mice were housed and bred at an American Association for the Accreditation of Laboratory Animal Care-accredited facility at NIH. The animal study proposal (LAD3E) was approved by the National Institute of Allergy and Infectious Diseases Animal Care and Use Committee.

Data Availability

Values for all data points in graphs are reported in the **Supporting Data Values** file. Whole genome sequencing data have been deposited to dbGAP (Accession #phs003261.v1.p1).

Author Contributions

AJA, WSC, ZX, AD performed experiments and analyzed and interpreted data. AZ provided cell lines and edited the paper. ARE and LAS recruited and cared for patients, performed skin testing and biopsies, and edited the paper. SMP analyzed and interpreted data and edited the paper. KMD supervised the project, performed experiments, analyzed and interpreted data, and wrote the paper. All authors read and approved the final manuscript.

Acknowledgements/Funding

This work was supported in part by the NIAID/NIH Intramural Program (Z01-AI-001083) to KMD. The content of this publication does not necessarily reflect the views or policies of the Department of Health and Human Services, nor does the mention of trade names, commercial products, or organizations imply endorsement by the U.S. Government. The funding body played no role in the design of the study and collection, analysis, and interpretation of data and in writing the manuscript. We thank Sundar Ganesan for assistance in confocal microscopy.

References

1. Eo TS, et al. Clinical Presentation, Management, and Prognostic Factors of Idiopathic Systemic Capillary Leak Syndrome: A Systematic Review. *J Allergy Clin Immunol Pract.* 2018;6(2):609-18.
2. Pineton de Chambrun M, et al. The Clinical Picture of Severe Systemic Capillary-Leak Syndrome Episodes Requiring ICU Admission. *Crit Care Med.* 2017;45(7):1216-23.
3. Xie Z, et al. High-dose intravenous immunoglobulin therapy for systemic capillary leak syndrome (Clarkson disease). *Am J Med.* 2015;128(1):91-5.

4. Pineton de Chambrun M, et al. Intravenous Immunoglobulins Improve Survival in Monoclonal Gammopathy-Associated Systemic Capillary-Leak Syndrome. *Am J Med.* 2017;130(10):1219 e19- e27.
5. Moyon Q, et al. Intravenous Immunoglobulins Tapering and Withdrawal in Systemic Capillary Leak Syndrome (Clarkson Disease). *J Allergy Clin Immunol Pract.* 2022;10(11):2889-95.
6. Pineton de Chambrun M, et al. SARS-CoV-2 Induces Acute and Refractory Relapse of Systemic Capillary Leak Syndrome (Clarkson's Disease). *Am J Med.* 2020;133(11):e663-e4.
7. Xie Z, et al. Neutrophil activation in systemic capillary leak syndrome (Clarkson disease). *Journal of cellular and molecular medicine.* 2019;23(8):5119-27.
8. Xie Z, et al. Markers of endothelial glycocalyx dysfunction in Clarkson disease. *J Transl Med.* 2022;20(1):380.
9. Druey KM, and Parikh SM. Idiopathic systemic capillary leak syndrome (Clarkson disease). *J Allergy Clin Immunol.* 2017;140(3):663-70.
10. Raza A, et al. A natural mouse model reveals genetic determinants of systemic capillary leak syndrome (Clarkson disease). *Commun Biol.* 2019;2:398.
11. Sek AC, X et al. Endothelial Expression of Endothelin Receptor A in the Systemic Capillary Leak Syndrome. *PLoS One.* 2015;10(7):e0133266.
12. Tyler AL, et al. Network-Based Functional Prediction Augments Genetic Association To Predict Candidate Genes for Histamine Hypersensitivity in Mice. *G3 (Bethesda).* 2019;9(12):4223-33.
13. Xie Z, et al. Genome-wide SNP analysis of the Systemic Capillary Leak Syndrome (Clarkson disease). *Rare Dis.* 2013;1(1).
14. Davalos D, et al. Fibrinogen-induced perivascular microglial clustering is required for the development of axonal damage in neuroinflammation. *Nat Commun.* 2012;3:1227.
15. Gao S, et al. Histamine induced high mobility group box-1 release from vascular endothelial cells through H(1) receptor. *Front Immunol.* 2022;13:930683.
16. Magro CM, Mo JH, and Pecker MS. Idiopathic systemic capillary leak syndrome, a unique complement and interferon mediated endotheliopathy syndrome: The role of the normal skin biopsy in establishing the diagnosis and elucidating pathogenetic mechanisms. *Ann Diagn Pathol.* 2022;61:152028.
17. Chang J, et al. Gpr124 is essential for blood-brain barrier integrity in central nervous system disease. *Nat Med.* 2017;23(4):450-60.
18. He S, et al. The protective effect of pericytes on vascular permeability after hemorrhagic shock and their relationship with Cx43. *Front Physiol.* 2022;13:948541.
19. Ratelade J, et al. Severity of arterial defects in the retina correlates with the burden of intracerebral haemorrhage in COL4A1-related stroke. *J Pathol.* 2018;244(4):408-20.
20. Mirando AC, et al. A collagen IV-derived peptide disrupts alpha5beta1 integrin and potentiates Ang2/Tie2 signaling. *JCI Insight.* 2019;4(4).
21. Xie Z, et al. Vascular endothelial hyperpermeability induces the clinical symptoms of Clarkson disease (the systemic capillary leak syndrome). *Blood.* 2012;119(18):4321-32.
22. Xie Z, et al. Mechanistic classification of the systemic capillary leak syndrome: Clarkson disease. *Am J Respir Crit Care Med.* 2014;189(9):1145-7.
23. Claesson-Welsh L, Dejana E, and McDonald DM. Permeability of the Endothelial Barrier: Identifying and Reconciling Controversies. *Trends Mol Med.* 2021;27(4):314-31.

24. Wang W, et al. Matrix stiffness regulates vascular integrity through focal adhesion kinase activity. *FASEB J.* 2019;33(1):1199-208.
25. Mathur T, et al. Vascular Transcriptomics: Investigating Endothelial Activation and Vascular Dysfunction Using Blood Outgrowth Endothelial Cells, Organ-Chips, and RNA Sequencing. *Curr Protoc.* 2022;2(10):e582.
26. Xie Z, et al. Inflammatory Markers of the Systemic Capillary Leak Syndrome (Clarkson Disease). *Journal of clinical & cellular immunology.* 2014;5:1000213.
27. Cai A, Chatziantoniou C, and Calmont A. Vascular Permeability: Regulation Pathways and Role in Kidney Diseases. *Nephron.* 2021;145(3):297-310.
28. Garcia V, and Sessa WC. Endothelial NOS: perspective and recent developments. *Br J Pharmacol.* 2019;176(2):189-96.
29. Vaz NM, et al. Sensitivity to intravenous injections of histamine and serotonin in inbred mouse strains. *Int Arch Allergy Appl Immunol.* 1977;53(6):545-54.
30. Hox V, et al.. Estrogen increases the severity of anaphylaxis in female mice through enhanced endothelial nitric oxide synthase expression and nitric oxide production. *J Allergy Clin Immunol.* 2015;135(3):729-36 e5.
31. Wang M, et al. The responses of pulmonary and systemic circulation and airway to anaphylactic mediators in anesthetized BALB/c mice. *Life Sci.* 2016;147:77-84.
32. Zhu D, et al. Magnesium Regulates Endothelial Barrier Functions through TRPM7, MagT1, and S1P1. *Adv Sci (Weinh).* 2019;6(18):1901166.
33. Stahmann N, et al. Activation of AMP-activated protein kinase by vascular endothelial growth factor mediates endothelial angiogenesis independently of nitric-oxide synthase. *J Biol Chem.* 2010;285(14):10638-52.
34. Dragoni S, et al. AMP-activated protein kinase is a key regulator of acute neurovascular permeability. *Journal of cell science.* 2021;134(7).
35. Gunduz D, et al. Compound C inhibits in vitro angiogenesis and ameliorates thrombin-induced endothelial barrier failure. *Eur J Pharmacol.* 2015;768:165-72.
36. Dasgupta B, and Seibel W. Compound C/Dorsomorphin: Its Use and Misuse as an AMPK Inhibitor. *Methods Mol Biol.* 2018;1732:195-202.
37. Fulton D, et al. Localization of endothelial nitric-oxide synthase phosphorylated on serine 1179 and nitric oxide in Golgi and plasma membrane defines the existence of two pools of active enzyme. *J Biol Chem.* 2002;277(6):4277-84.
38. Haeussler DJ, et al. Endomembrane H-Ras controls vascular endothelial growth factor-induced nitric-oxide synthase-mediated endothelial cell migration. *J Biol Chem.* 2013;288(21):15380-9.
39. Holton M, et al. Endothelial nitric oxide synthase activity is inhibited by the plasma membrane calcium ATPase in human endothelial cells. *Cardiovascular research.* 2010;87(3):440-8.
40. Luo Y, et al. Roles of I(2)(PP2A) in the downregulation of eNOS Ser1177 phosphorylation by angiotensin II-activated PP2A. *Biochem Biophys Res Commun.* 2019;516(3):613-8.
41. Lacroix B, Lorca T, and Castro A. Structural, enzymatic and spatiotemporal regulation of PP2A-B55 phosphatase in the control of mitosis. *Front Cell Dev Biol.* 2022;10:967909.
42. Hacke M, et al. Inhibition of Ebola virus glycoprotein-mediated cytotoxicity by targeting its transmembrane domain and cholesterol. *Nat Commun.* 2015;6:7688.

43. Ghosh CC, et al. Gene control of tyrosine kinase TIE2 and vascular manifestations of infections. *Proc Natl Acad Sci U S A.* 2016;113(9):2472-7.
44. Parikh SM. Targeting Tie2 and the host vascular response in sepsis. *Sci Transl Med.* 2016;8(335):335fs9.
45. Ozkan M, et al. Variants in TNF and NOS3 (eNOS) genes associated with sepsis in adult patients. *J Gene Med.* 2021;23(4):e3323.
46. Pierce RW, et al. A p190BRhoGAP mutation and prolonged RhoB activation in fatal systemic capillary leak syndrome. *The Journal of experimental medicine.* 2017;214(12):3497-505.
47. Pierce R, et al. Whole-Exome Sequencing of Adult and Pediatric Cohorts of the Rare Vascular Disorder Systemic Capillary Leak Syndrome. *Shock.* 2019;52(2):183-90.
48. Ninchoji T, et al. eNOS-induced vascular barrier disruption in retinopathy by c-Src activation and tyrosine phosphorylation of VE-cadherin. *Elife.* 2021;10.
49. Zhang Q, et al. Functional relevance of Golgi- and plasma membrane-localized endothelial NO synthase in reconstituted endothelial cells. *Arterioscler Thromb Vasc Biol.* 2006;26(5):1015-21.
50. Fernandez-Hernando C, et al. Genetic evidence supporting a critical role of endothelial caveolin-1 during the progression of atherosclerosis. *Cell Metab.* 2009;10(1):48-54.
51. Chen W, et al. Cancer-associated PP2A Aalpha subunits induce functional haploinsufficiency and tumorigenicity. *Cancer Res.* 2005;65(18):8183-92.
52. Taylor SE, et al. The Highly Recurrent PP2A Aalpha-Subunit Mutation P179R Alters Protein Structure and Impairs PP2A Enzyme Function to Promote Endometrial Tumorigenesis. *Cancer Res.* 2019;79(16):4242-57.
53. Atkinson JP, et al. Systemic capillary leak syndrome and monoclonal IgG gammopathy; studies in a sixth patient and a review of the literature. *Medicine (Baltimore).* 1977;56(3):225-39.
54. Cheung P, et al. Fatal Exacerbations of Systemic Capillary Leak Syndrome Complicating Coronavirus Disease. *Emerging Infectious Disease journal.* 2021;27(10).
55. Umbrello M, et al. Systemic capillary leak syndrome: is methylene blue the silver bullet? *Case Rep Crit Care.* 2014;2014:141670.
56. Chen S, et al. fastp: an ultra-fast all-in-one FASTQ preprocessor. *Bioinformatics.* 2018;34(17):i884-i90.
57. Faust GG, and Hall IM. SAMBLASTER: fast duplicate marking and structural variant read extraction. *Bioinformatics.* 2014;30(17):2503-5.
58. Danecek P, et al. Twelve years of SAMtools and BCFtools. *Gigascience.* 2021;10(2).
59. Poplin R, et al. A universal SNP and small-indel variant caller using deep neural networks. *Nat Biotechnol.* 2018;36(10):983-7.
60. Yun T, L et al. Accurate, scalable cohort variant calls using DeepVariant and GLnexus. *Bioinformatics.* 2021;36(24):5582-9.
61. Karczewski KJ, et al. The mutational constraint spectrum quantified from variation in 141,456 humans. *Nature.* 2020;581(7809):434-43.
62. Rentzsch P, et al. CADD: predicting the deleteriousness of variants throughout the human genome. *Nucleic acids research.* 2019;47(D1):D886-D94.
63. Pagel KA, et al. Integrated Informatics Analysis of Cancer-Related Variants. *JCO Clin Cancer Inform.* 2020;4:310-7.

64. Sevim Bayrak C, et al. Identification of discriminative gene-level and protein-level features associated with pathogenic gain-of-function and loss-of-function variants. *American journal of human genetics.* 2021;108(12):2301-18.

Figures and Legends

Fig 1

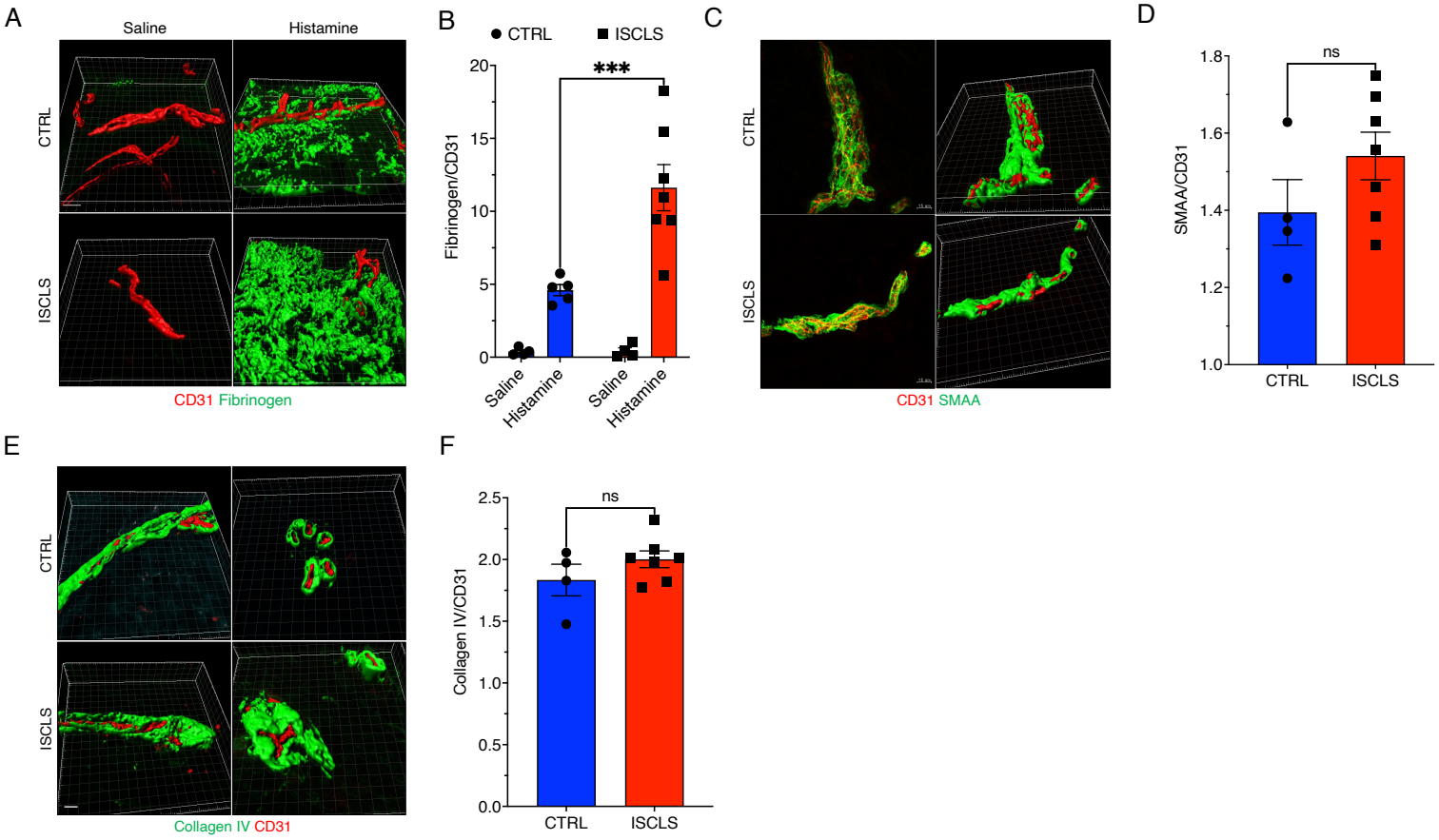

Figure 1 Increased histamine-induced vascular leakage in ISCLS skin. (A) 3D rendering of fibrinogen (green) and CD31 (red) immunostaining in representative skin biopsies obtained after intradermal challenge with saline or histamine. Scale bar=10 µm; original magnification 63x. **(B)** Ratio of fibrinogen/CD31 area (µm^2); mean ± s.e.m. of n=7 ISCLS, 5 controls (CTRL), ***p=0.0006, 2-way ANOVA, Sidak multiple comparisons. **(C-D)** α-smooth muscle actin (SMAA, green) or CD31 (red) immunostaining (left panels) and 3D rendering (right panels) in representative skin biopsies (C) and SMAA/CD31 ratio quantified (D); mean ± s.e.m. of n=4 ISCLS, 7 CTRL, ns=not significant, unpaired t test. Scale bar=10 µm; original magnification 63x. **(E-F)** Collagen type IV (green) or CD31 (red) immunostaining (left panels) in representative skin biopsies (E) and collagen IV/CD31 ratio quantified (F); mean ± s.e.m. of n=4 ISCLS, 7 CTRL, ns=not significant, unpaired t test. Scale bar=10 µm; original magnification 63x.

Fig 2

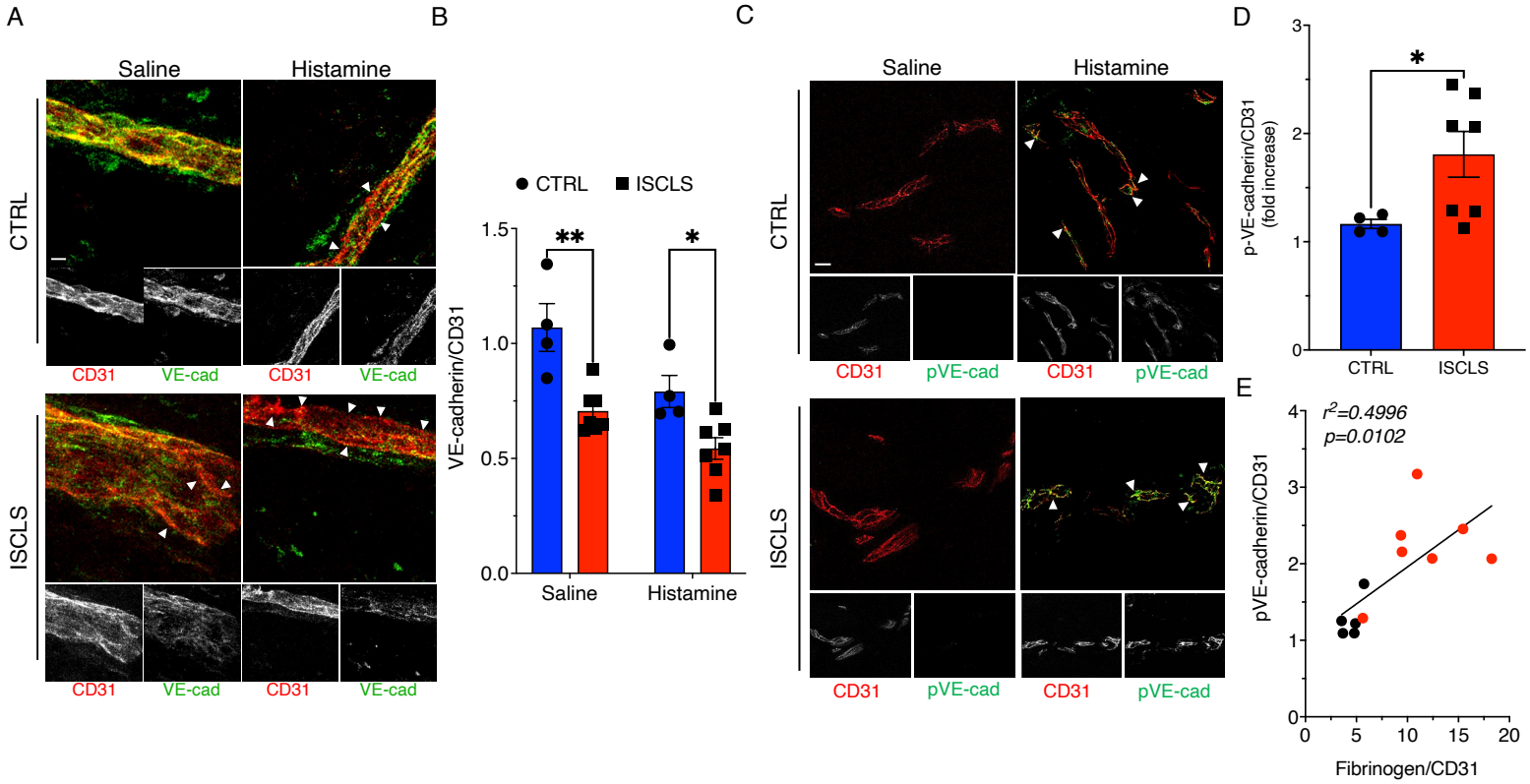

Figure 2 Adherens junction protein expression in dermal microvasculature. (A) VE-cadherin (green) or CD31 (red) immunostaining in representative skin biopsies; arrowheads indicate areas of decreased VE-cadherin expression (red), which is reflected in black/white panels of individual immunostains (lower panels) **(B)** Ratio of VE-cadherin/CD31 immunostaining; mean ± s.e.m. of n=4 CTRL, 7 ISCLS, **p*=0.01, ***p*=0.001, 2-way ANOVA, Sidak multiple comparisons. **(C)** Phospho-VE-cadherin^{Tyr685} (green, arrowheads) and CD31 (red) immunostaining in representative skin biopsies; black/white panels show corresponding individual stains as indicated. **(D)** Phospho-VE-cadherin/CD31 immunostaining (μm^2) in histamine-challenged skin biopsies (mean ± s.e.m. of n=4 CTRL, 7 ISCLS, **p*=0.02, Mann-Whitney. **(E)** Pearson correlation of phospho-VE-cadherin immunostaining with fibrinogen extravasation. Scale bars=10 µm; original magnification 63x.

Fig 3

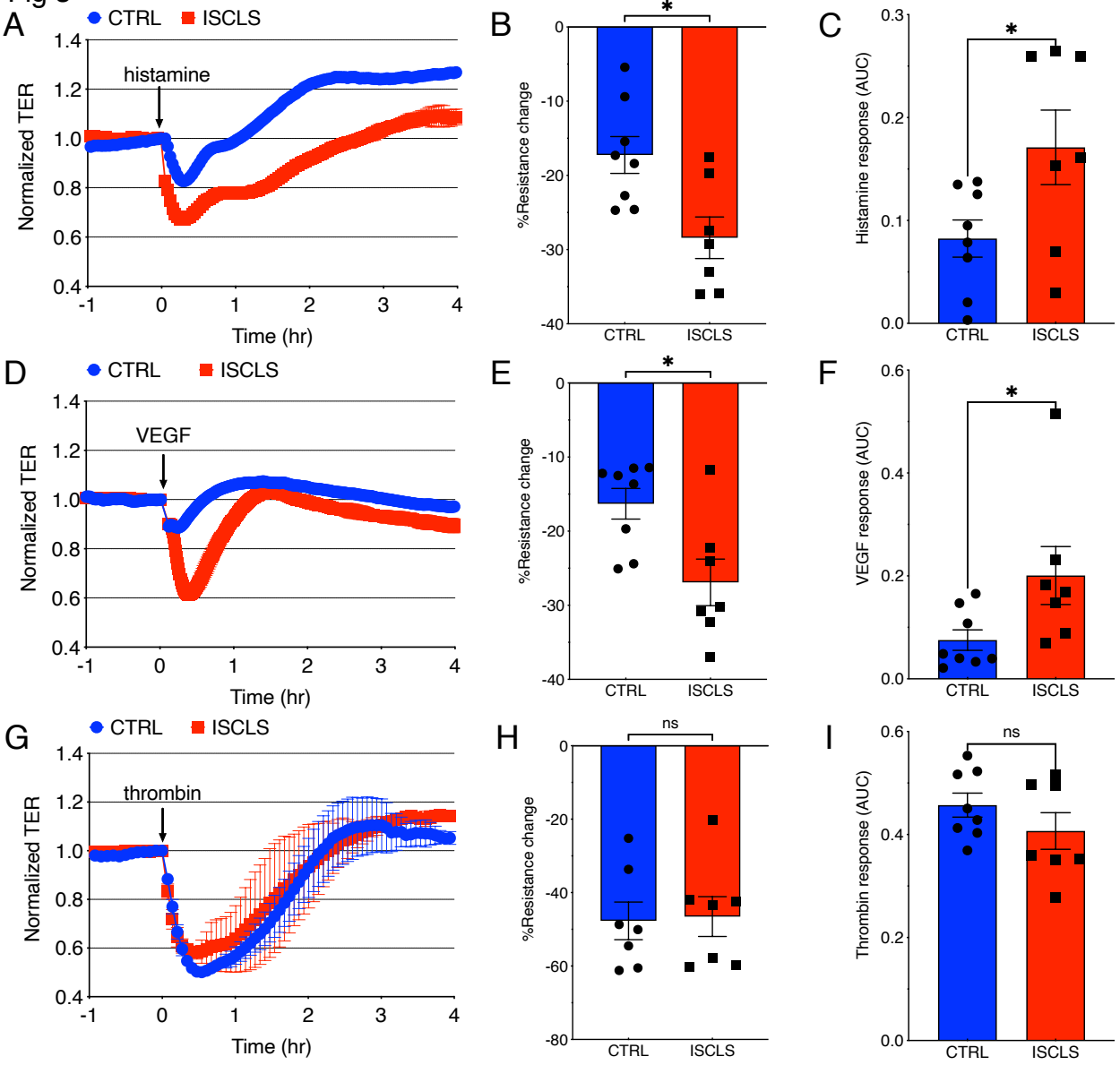

Figure 3 Hyper-responsiveness of ISCLS-derived ECs in vitro. Representative trans-endothelial resistance (TER) over time in blood-outgrowth endothelial cell (BOEC) monolayers stimulated with histamine (20 μM) **(A)**, VEGF (100 ng/mL) **(D)**, or thrombin (0.05 U/mL) **(G)**; mean ± S.D.; arrows indicated time of agonist addition. **(B, E, H)** Maximum decrease in TER elicited by respective agonists; mean ± s.e.m. of n=8 CTRL, 7 ISCLS, **p*=0.01, unpaired *t* test. **(C, F, I)** Area under curve (AUC) for each agonist; mean ± s.e.m. of n=8 CTRL, 7 ISCLS, **p*=0.04, unpaired *t* test (C); **p*=0.01, Mann Whitney (F).

Fig 4

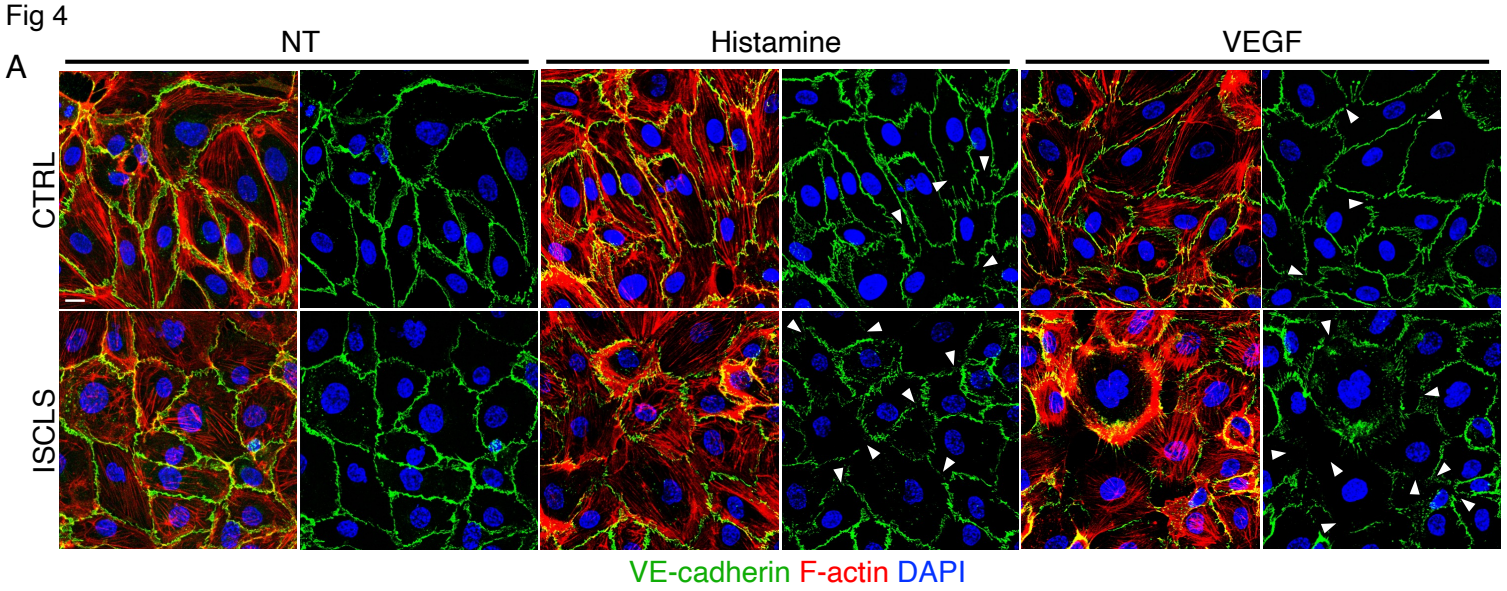

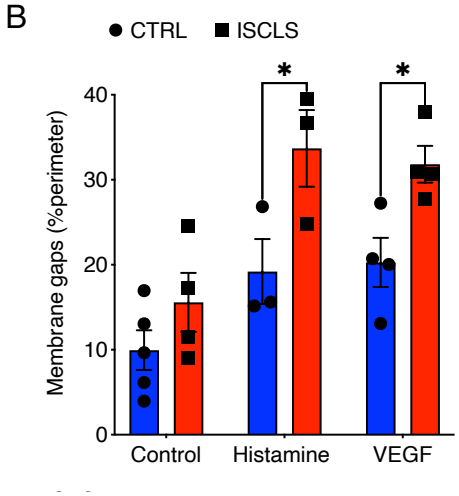

Figure 4 Structural correlates of impaired barrier function in BOECs. (A) Representative images of BOECs at homeostasis (non-treated, NT) or stimulated with histamine (20 μM) or VEGF (100 ng/mL) for 15 minutes and stained with VE-cadherin antibody (green), phalloidin (red), and DAPI (blue); arrowheads indicate areas of membrane disruption. Scale bar 15 μm, original magnification 63x. **(B)** Quantification of membrane disruption as a percentage of cell perimeter; mean ± s.e.m. of n=2-3 donors/group analyzed in 3-5 independent experiments, *p<0.04, 2-way ANOVA, Sidak multiple comparisons.

Fig 5

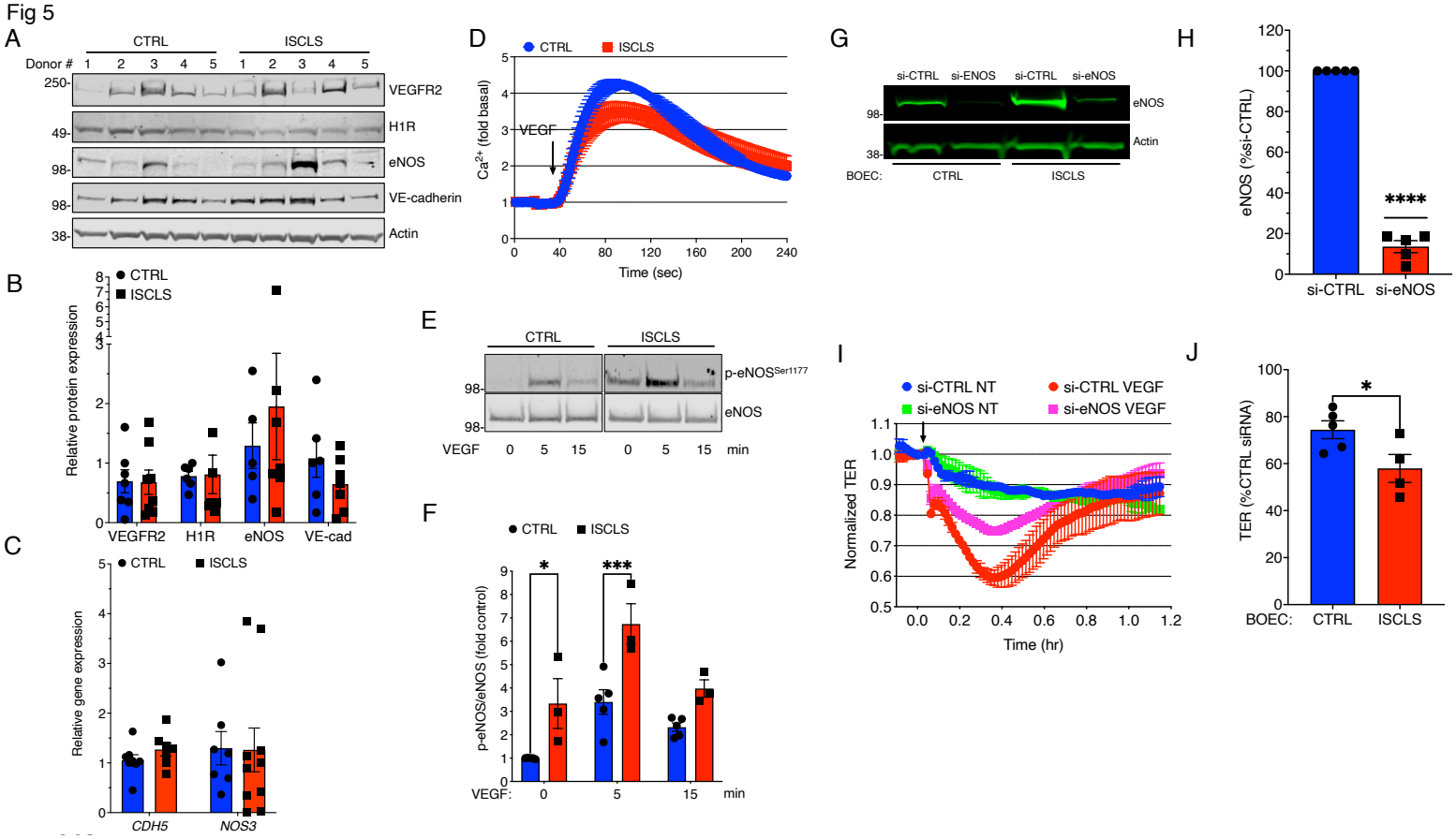

Figure 5 Hyper-responsiveness of ISCLS BOECs is eNOS-dependent. (A) Representative immunoblot of relevant receptors or signaling proteins in BOEC cell lysates (n=5 donors/group). (**B**) Quantification of relative protein expression. Mean ± s.e.m. of n=6-9 donors/group; ns, 2-way ANOVA, Sidak multiple comparisons. **(C)** Relative *CDH5* or *NOS3* expression in BOECs evaluated by qPCR (normalized by *Actb* and/or *GAPDH*). Mean ± s.e.m. of n=6-10 donors/group; ns, Mann Whitney. **(D)** Relative intracellular Ca^{2+} concentrations in CTRL (blue) or ISCLS-derived (red) BOECs stimulated with VEGF (100 ng/mL); mean ± s.e.m. of n=2-3 donors/group analyzed in 4-5 independent experiments. **(E)** Representative immunoblot phospho-eNOS^{Ser1177} and total eNOS in lysates from BOECs stimulated with VEGF and immunoprecipitated with eNOS antibody. **(F)** p-eNOS/eNOS quantified; mean ± s.e.m. of 3-5 donors/group analyzed in 5 independent experiments, *p=0.01, ***p=0.0008, 2-way ANOVA, Sidak multiple comparisons. **(G-H)** Representative immunoblot (F) and quantification (G) of eNOS/actin in eNOS siRNA transfected BOECs; mean ± s.e.m. of 5 independent experiments, ****p<0.0001, 1 sample t test. **(I)** Representative TER in control or eNOS siRNA transfected BOECs left untreated (blue and green) or stimulated with VEGF (red and magenta). **(J)** Maximum decrease in VEGF-induced TER from t=0 as a percentage of the control siRNA response; mean ± s.e.m. of n=4-5 donors/group analyzed in 3-5 independent experiments, *p=0.04, unpaired t test.

Fig 6

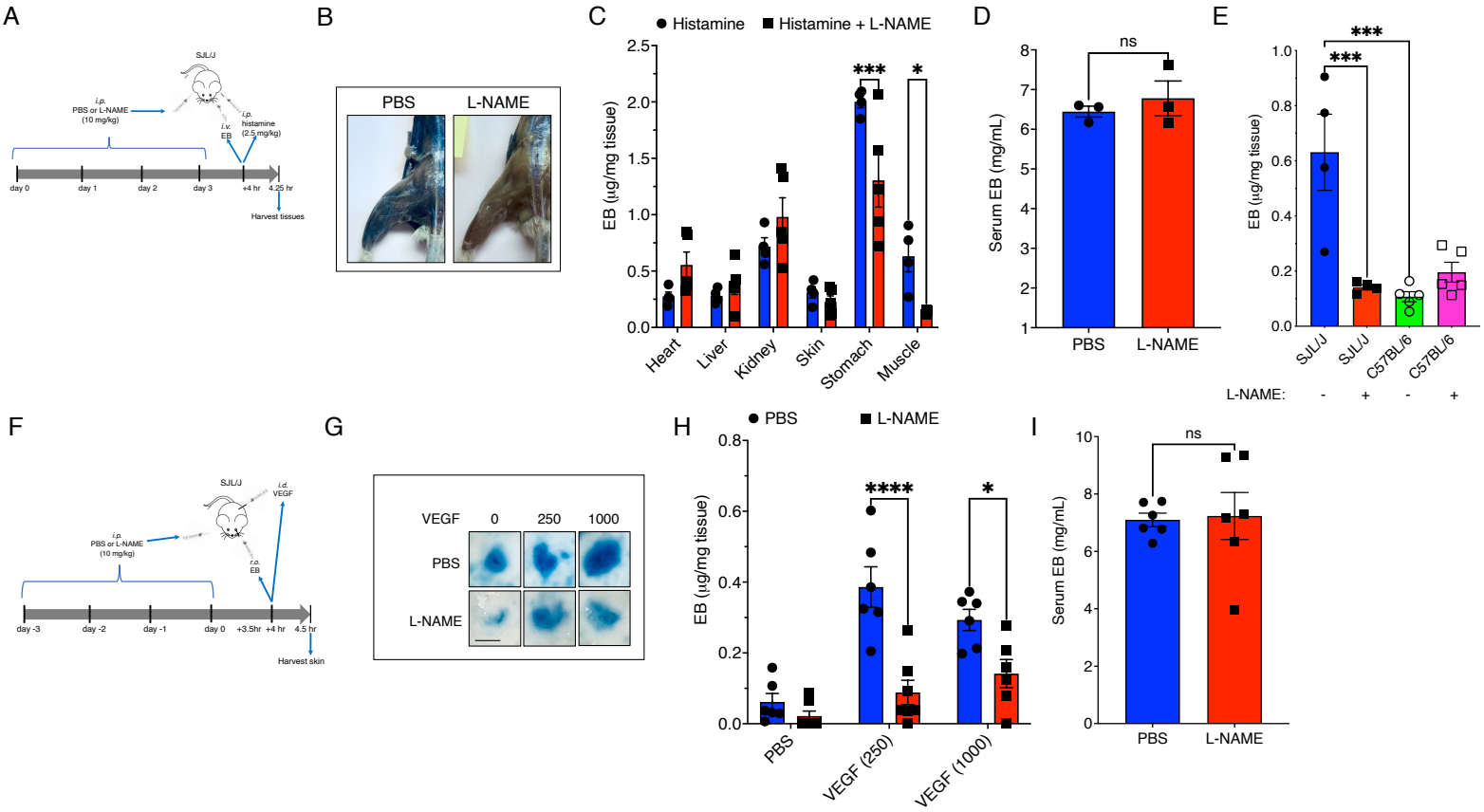

Figure 6 Effect of eNOS blockade in a mouse model of ISCLS. (A) Analysis of histamine-induced systemic vascular leakage in SJL/J mice. **(B)** Representative images of EB extravasation in legs of mice pretreated with L-NAME (10 mg/kg) or PBS and challenged with histamine (2.5 mg/kg) intraperitoneally (i.p.). **(C-D)** Relative EB quantities in organs (C) or serum (D) from SJL/J mice challenged with histamine systemically; mean ± s.e.m. of n=3-5 mice/group, **p*=0.04, ****p*=0.001, 2-way ANOVA, Sidak multiple comparisons (C), ns, Mann-Whitney (D). **(E)** EB content in muscle from respective mice pretreated or not with L-NAME and challenged with histamine systemically. Mean ± s.e.m. of n=4-5 mice/group, ****p*<0.0009, 1-way ANOVA, Tukey multiple comparisons. **(F)** Analysis of vascular leakage in skin following intradermal challenge with VEGF. **(G)** Representative images of EB in skin challenged as indicated. **(H-I)** Relative EB quantities in skin (H) or serum (I) of mice challenged with VEGF intradermally; mean ± s.e.m. of n=6-7 mice/group, **p*=0.01, *****p*<0.0001, 2-way ANOVA, Sidak multiple comparisons (H), ns, Mann Whitney (I). Scale bar=5 µm.

Fig 7

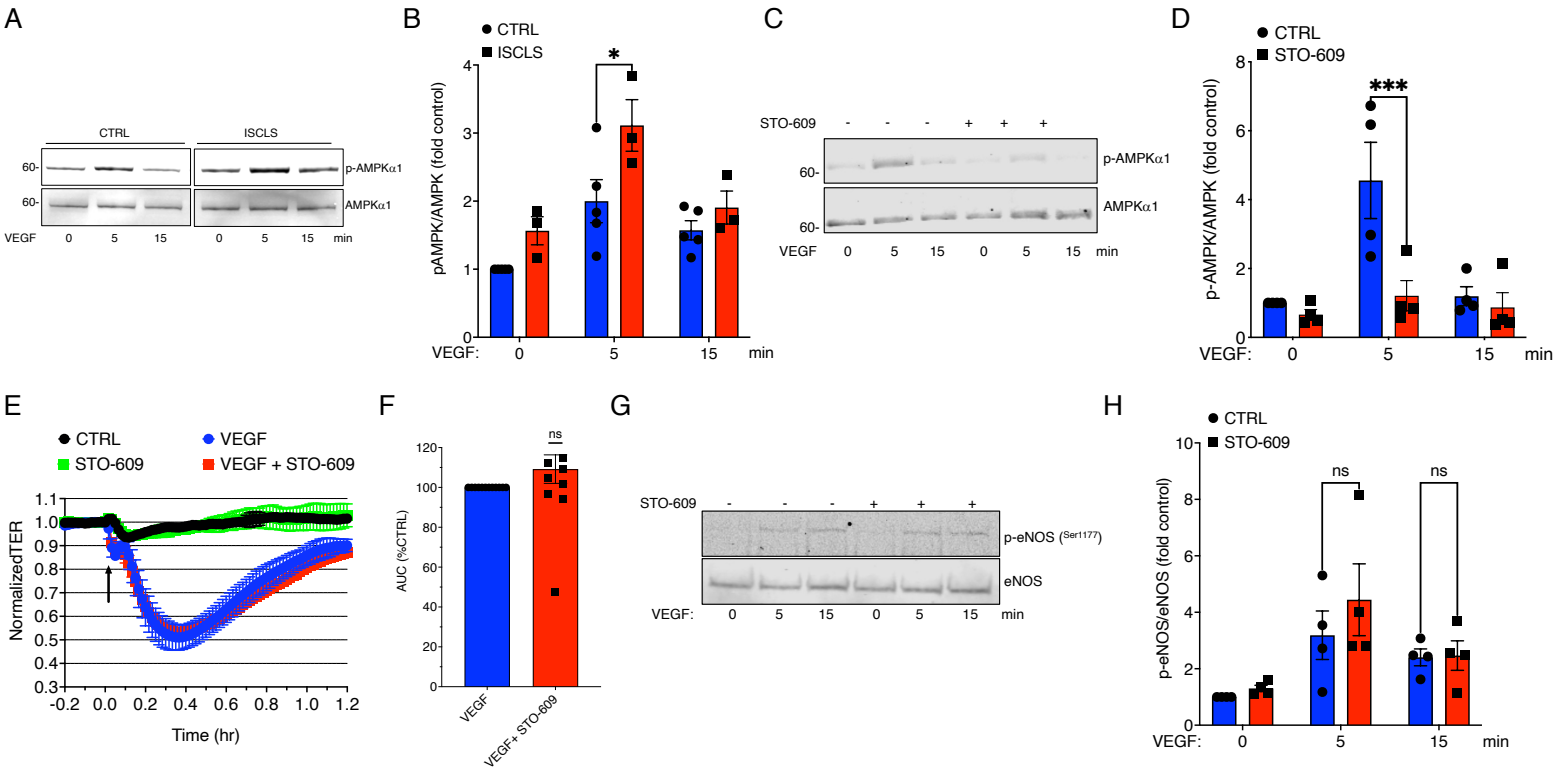

Figure 7 Role of AMPK in eNOS hyper-phosphorylation in ISCLS-derived BOECs. (A-B) Representative blot (A) and quantification (B) of pAMPK/AMPK in BOECs left untreated or stimulated with VEGF (100 ng/mL) (B); mean ± s.e.m. of n=3-4 donors/group, *p=0.01, 2-way ANOVA, Sidak multiple comparisons. **(C-D)** Representative blot (C) and quantification (D) of pAMPK/AMPK in BOECs pretreated with STO-609 (12 µM for 6 hours) or vehicle and stimulated with VEGF (100 ng/mL) for the indicated times; mean ± s.e.m. of n=2 donors/group analyzed in 4 independent experiments, ***p=0.0009, 2-way ANOVA, Sidak multiple comparisons. **(E-F)** TER (E) and AUC (F) in BOECs pretreated with vehicle or STO-609; n=2 donors/group analyzed in 4 independent experiments, ns, 1-sample *t* test. **(G-H)** Representative blot (G) and quantification (H) of p-eNOS/eNOS in BOECs pretreated with STO-609 or vehicle and stimulated with VEGF (100 ng/mL) for the indicated times; mean ± s.e.m. of n=2 donors/group analyzed in 4 independent experiments, ns, 2-way ANOVA, Tukey multiple comparisons. (G) Representative blot (G) and quantification (H) of p-eNOS/eNOS in BOECs left untreated or pretreated with STO-609 and stimulated with VEGF (100 ng/mL); mean ± s.e.m. of n=3-4 donors/group; ns, 2-way ANOVA, Tukey multiple comparisons.

Fig 8

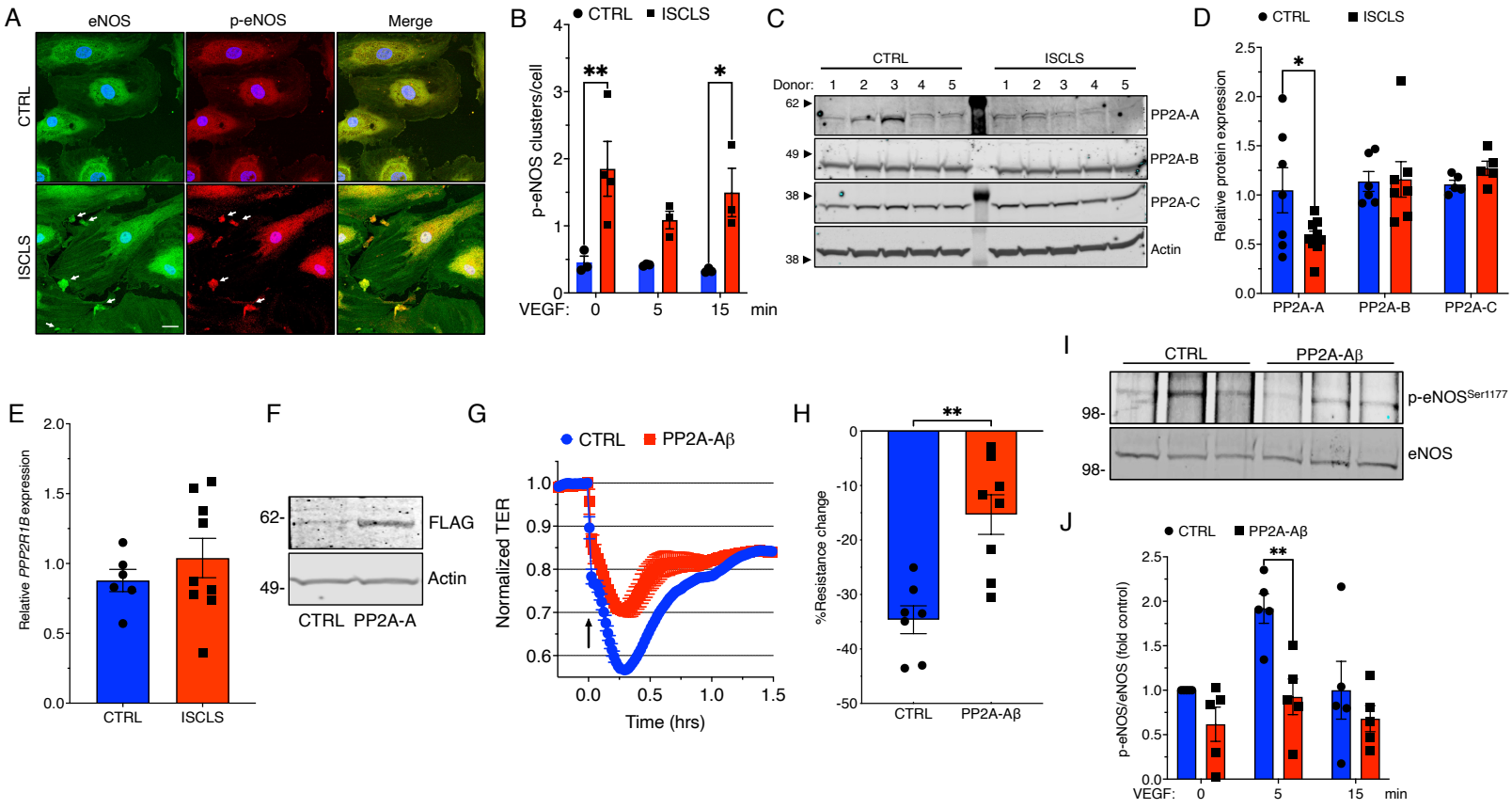

Figure 8 Aberrant eNOS localization and PP2A expression in ISCLS-derived BOECs. (A) BOECs stained with phospho-eNOS (left, green) or eNOS (middle, red) antibodies and DAPI. Arrows denote eNOS clusters. Scale bar=20 µm. **(B)** Numbers of eNOS clusters/cell; mean ± s.e.m. of n=3 cell lines/group; *p=0.03, **p=0.006, 2-way ANOVA, Sidak multiple comparisons. **(C)** Representative immunoblot of PP2A subunits in BOEC cell lysates (n=5 donors/group). **(D)** Quantification of relative protein expression. Mean ± s.e.m. of n=7-9 donors/group; *p=0.03, 2-way ANOVA, Sidak multiple comparisons. **(E)** Relative *PPP2R1B* expression in BOECs evaluated by qPCR (normalized by *GAPDH*). Mean ± s.e.m. of n=6-9 donors/group; ns, unpaired *t* test. **(F)** Representative immunoblot of FLAG-PP2A-Aβ in BOECs transfected with respective lentiviruses. **(G-H)** Representative TER (G) and maximum decrease in VEGF-induced TER (H) from t=0 (arrow) in BOECs infected with control or FLAG-PP2A-β encoding lentivirus; mean ± s.e.m. of n=2 donors/group analyzed in 4 independent experiments, **p=0.001, unpaired *t* test. **(I-J)** Representative blot (I) and quantification (J) of p-eNOS/eNOS in control vs. FLAG-PP2A-β overexpressing BOECs stimulated with VEGF (100 ng/mL); mean ± s.e.m. of n=5 independent experiments. **p=0.004, 2-way ANOVA, Sidak multiple comparisons.

953